Dynamics of Small, Ultraviolet-Excited ICN⁻ Cluster Anions

Amanda S. Case,[†,§] Anne B. McCoy,*[,‡] and W. Carl Lineberger*[,†]

[†]JILA and Department of Chemistry and Biochemistry, University of Colorado at Boulder, Boulder, Colorado 80309, United States
[‡]Department of Chemistry and Biochemistry, The Ohio State University, Columbus, Ohio 43210, United States

Ⓢ Supporting Information

ABSTRACT: The ultraviolet (UV) photodissociation of mass-selected ICN^-Ar_n and $ICN^-(CO_2)_n$ clusters ($n = 0-5$) is studied using a secondary reflectron mass spectrometer. Relative photodissociation cross sections of bare ICN^- show the dominance of the I^- photoproduct from 270 to 355 nm, the entire wavelength range studied. UV excitation populates both the $^2\Sigma^+$ state that produces $I^* + CN^-$ and the $^2\Pi$ states that produce $I^- + CN^*$. While the excited $^2\Pi$ states directly

$$h\nu + ICN^-(S)_n \longrightarrow \begin{cases} CN^-(S)_x + I \text{ or } I^* + (n-x)S \\ I^-(S)_y + CN \text{ or } CN^* + (n-y)S \\ ICN^-(S)_z + (n-z)S \end{cases}$$

produce I^-, excitation to the $^2\Sigma^+$ state also produces some I^- product via nonadiabatic transitions to the $^2\Pi_{1/2}$ state, which produces $I^- + CN$. Partial solvation of the anion by Ar atoms or CO_2 molecules alters the UV-branching percentages between the various dissociation channels: $I^* + CN^-$ and $I^- + CN$ or $I^- + CN^*$. In addition, solvation by two or more Ar atoms or three or more CO_2 molecules results in recombination, reforming ICN^-. Examination of the potential surfaces and transition moments in combination with the results of quantum dynamics calculations performed on the relevant excited states assist in the analysis of the experimental results.
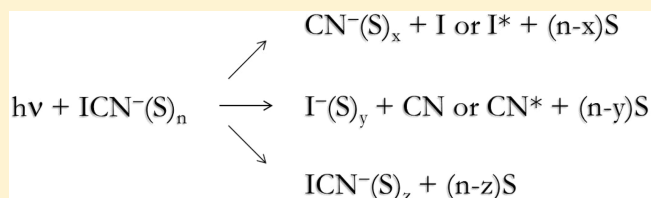
I. INTRODUCTION

As not only a triatomic but also a linear molecule, ICN appears deceptively simple. Yet, studies of neutral ICN are extensive, revealing dynamics complicated by the presence of a conical intersection. The review by Black et al. and references therein provide an excellent overview of the photochemistry of ICN.[1] The 266-nm excitation of ICN to the A continuum produces a bimodal rotational distribution in the CN product, and this bimodal nature is the result of two product channels: $I(^2P_{3/2}) + CN(^2\Sigma^+)$, $\langle E_{rot} \rangle = 0.41$ eV and $I^*(^2P_{1/2}) + CN(^2\Sigma^+)$, $\langle E_{rot} \rangle = 0.04$ eV.[2] These two contrasting product channels were believed to be due to the presence of a conical intersection, and, indeed, trajectory calculations that were run on accurate potential-energy surfaces[3,4] established that bending motion, which occurs along with the I−CN bond elongation, maps into torque on the CN as ICN passes through a conical intersection. This torque produces highly rotationally excited CN along with the $I(^2P_{3/2})$ cofragment. Further studies done in the condensed phase[5,6] show the persistence of the CN rotation, as the nonadiabatic channel produces highly rotationally excited CN even in the presence of strongly interacting solvents.

Recent studies on the photodissociation of ICN⁻ indicate, yet again, a highly rotationally excited CN fragment.[7] This high degree of CN rotation serves as a major sink for internal energy and is important in the intramolecular energy flow pathways. The CN rotor facilitates quasi-thermionic electron emission by allowing the photoexcited anion to serve as its own heat bath. In the 500-nm photodissociation of ICN⁻Ar, the ability of the anion to sequester substantial amounts of energy in CN rotation as it dissociates enables recombination of ICN⁻ with even a single Ar atom. Additionally, the sizable amount of energy tied up by CN rotation from the visible photo-

dissociation of small clusters of ICN⁻ with Ar results in the production of Ar-solvated recombined photoproducts despite the fact that the available energy is in excess of the Ar binding energy. These recombined anions, both bare and solvated, are believed to re-form via a radiative mechanism.

While the Ar-solvated ICN⁻ visible photodissociation results are surprising, the visible photodissociation dynamics of ICN⁻ clusters formed with a CO_2 solvent[8] follows more closely with previous dihalide studies.[9−12] Photofragmentation of $ICN^-(CO_2)_n$ using 500-nm light produces predominantly CN⁻-based photoproducts ($n = 2-18$) and recombination is not observed until $n = 2$. The degree of solvation of the recombined ICN⁻-based photoproducts also follows the evaporative ensemble[13] model, as has been seen with I_2^-,[10] ICl⁻,[9] and IBr⁻,[11,12] demonstrating that recombination of $ICN^-(CO_2)_n$ occurs via a nonadiabatic transition to the ground state.[8] However, unlike IBr⁻ and ICl⁻, for ICN⁻ the formation of CN⁻-based, charge-transfer products is strongly driven by the ability of $CN^-(CO_2)$ to form the molecular anion $[NCCO_2]^-$.[8,14]

Figure 1a shows a schematic representation of the potential-energy curves for linear ICN⁻ adapted from Martin et al.[8] and McCoy.[15] The $^2\Sigma^+$-(X) state is shown in red and the blue, green, and purple curves represent optically accessible excited states; the black state is optically dark. In this figure and throughout the paper, the linear state labeling refers to the
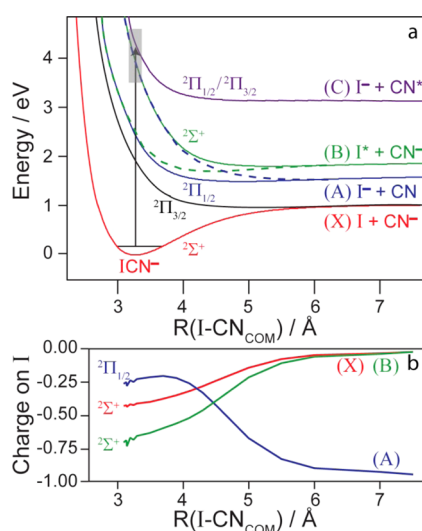
Figure 1. (a) Potential-energy curves (based on refs 8 and 15) for linear ICN⁻ as a function of the I−CN$_{COM}$ distance. The solid curves are the adiabatic potentials for the $^2\Sigma^+$-(X) ground state (red), the $^2\Pi_{1/2}$-(A) excited state (blue), the $^2\Sigma^+$-(B) excited state (green), and the $^2\Pi$-(C) excited states (purple); the $^2\Pi_{3/2}$-(A) excited state (black) is optically dark. The blue and green dashed curves represent diabatic states based on the electronic structure calculations. The arrow illustrates photoexcitation of the anion using 300-nm light, while the gray band shows the excitation range used to determine the relative photodissocation cross section: 270 to 355 nm . (b) Calculated charge on the I atom as a function of the I-CN$_{COM}$ separation for the $^2\Sigma^+$-(X), $^2\Pi_{1/2}$-(A), and $^2\Sigma^+$-(B) excited states of bare ICN⁻.

initially excited state, and the alphabetized state label denotes the asymptotic products. The black arrow in Figure 1a corresponds to 300-nm (4.1-eV) excitation, while the gray box shows the 277- to 355-nm wavelength region over which the relative photodissociation cross sections are obtained. By analogy to the diatomic dihalides, where the strongest electronic transition is from the ground state to the $^2\Sigma^+$-excited state,[16] the dominant ionic photoproduct is expected to be CN⁻. The expected dominance of CN⁻ assumes that in ICN⁻, the excitation is also primarily to the $^2\Sigma^+$ state and the anion dissociates on this adiabatic potential (solid green curve in Figure 1a). Whereas the solid curves shown in Figure 1a are adiabatic potentials for linear ICN⁻, the dashed lines represent the results of a diabatization based on the electronic structure calculations.[8] In the case of visible excitation of bare ICN⁻ using 500-nm (2.5-eV) light, if the dynamics followed the adiabatic potential the only ionic product would be I⁻; however, because of the interaction of the $^2\Pi_{1/2}$-(A) and $^2\Sigma^+$-(B) states, CN⁻ accounts for roughly 3% of the observed ionic photoproducts.[8] A similar nonadiabatic mechanism is expected to play a larger role in the dynamics following excitation in the UV. For UV excitation it is also possible that the ICN⁻ is excited to the nearby degenerate pair of $^2\Pi$-(C) states, which produce I⁻ + CN*. While the transition strength for excitation to these states is expected to be small in the equilibrium linear ICN⁻ geometry, the anion undergoes large amplitude bending vibrations.[8] The lowered symmetry of bent ICN⁻ leads to the expectation of an increase in the importance of the $^2\Pi$-(C) states in the dynamics. Both of the above mechanisms provide an opportunity for I⁻ to represent a significant fraction of the photoproducts following UV excitation of ICN⁻.

Herein, we explore the photodissociation dynamics of both bare and partially solvated ICN⁻ following UV excitation. Surprisingly, the dominant ionic photoproduct detected from UV photodissociation of ICN⁻ is I⁻. From the determination of the photodissociation cross section, we find a maximum near 300 nm and at this wavelength obtain branching percentages for ICN⁻; ICN⁻Ar$_n$, n = 1−5; and ICN⁻(CO$_2$)$_n$, n = 1−5. We use quantum dynamics calculations to confirm the role of nonadiabatic dissociation in bare ICN⁻ and to clarify the experimental findings of the photodissociation of partially solvated ICN⁻.

II. METHODS

A. Experiment. A complete description of the experimental apparatus used for these studies has been previously published.[9,17,18] Here we briefly describe the anion formation, mass selection, and photoproduct detection using a reflectron mass spectrometer.

We synthesize solid ICN using the procedure reported by Bak and Hillebert.[19] Neat Ar (20−30 psig) or CO$_2$ (15−25 psig) passes over solid ICN and then expands from a 0.8-mm orifice of a pulsed General Valve nozzle into the ion-source chamber. The expanding gas encounters a focused and guided 1-keV electron beam forming a variety of ions. A Wiley−McLaren time-of-flight mass spectrometer (TOF MS)[20] extracts the anions, where they separate by their mass-to-charge ratio. While in the TOF MS, a fast potential switch rereferences the anions to ground potential and an einzel lens focuses the anions into the interaction region. A mass gate, located just prior to the anion spatial focus, selects the desired anion and allows only this single species into the interaction region.

The doubled output of a Nd:YAG-pumped optical parametric oscillator is collimated into the interaction region. The photoproducts generated from the anion-light interaction enter a single-stage secondary reflectron mass spectrometer. The reflectron separates the anionic photoproducts by mass, and a dual set of microchannel plates detects the photoproducts 8° off of the axis of the parent-ion beam. Changing the potential applied to the reflectron allows different anionic products to impinge upon the detector; an oscilloscope collects the signal from the detector for various potentials, thereby permitting detection of all anionic photoproducts.

Each data set acquired contains both signal (laser and ion beams overlapped in time) and background (laser and ion beams not overlapped in time) traces of the parent ion as well as all photoproducts, where each trace is the average of 128 laser shots. These traces are then digitized, and a small background subtraction is performed. The integral of the parent ion signal, A(parent) and of each photoproduct ion, A(i), is then determined. The laser power P is separately determined. These quantities are used to determine the relative photodissociation cross section for each product using the relation

$$\sigma_{i,rel}(\lambda) = \frac{A_i/d_i}{P\lambda[A(\text{parent ion})/d_{\text{parent}}]}k_{\text{apparatus}} \qquad (1)$$

where d_i is the detection efficiency of product ion of type i, d_{parent} is the detection efficiency of the parent ion, and $k_{\text{apparatus}}$ is a constant that contains all of the measured and unmeasured experimental parameters (such as ion beam-laser beam overlap) that are independent of the identity of the product ion being measured. The factor d_{parent} is common to all partial cross

sections and can be considered to be incorporated into $k_{apparatus}$. Separate measurements demonstrated that the product-ion detector is operating in a saturated gain mode such that the detection efficiency d_i of each product ion is roughly the same. The factor λ is required to convert laser power into a quantity proportional to the number of photons. For the photodissociation cross section shown, each point is the average of 10 data sets.

To determine the photoproduct branching percentages ($\%_i$), where the indices i and k refer to the photoproducts, we utilize

$$\%_i(\lambda) = 100 \frac{\sigma_{i,rel}(\lambda)}{\sum_{k=1}^{n} \sigma_{k,rel}(\lambda)} = 100 \frac{A_i}{\sum_{k=1}^{n} A_k} \qquad (2)$$

We report the average of 20 data sets. (The percentages and standard deviations given for bare ICN^- are from data taken following expansion in Ar (20 sets) and CO_2 (5 sets); the 5 data sets taken for expansion with CO_2 were obtained to ensure that the branching was the same for the two different carrier gases.)

B. Theory. The theoretical aspects of this study consist of three parts. The first, involves the development of potential-energy surfaces for the ground and accessed excited states of ICN^-. The second, requires the evaluation of the photodissociation dynamics and product-state distributions based on these potentials. The third, involves using our knowledge of these potentials to anticipate the effects of solvation of the anion with Ar or CO_2 on the dynamics, which aids in the interpretation of some of the experimental findings.

To start, we consider the potential-energy surfaces. As noted in previous studies involving the adiabatic potentials, the electronic structure of ICN^- changes dramatically at an I−CN_{COM} separation of approximately 4.5 Å.[15] This can be seen, in Figure 1b, by comparing the charge on the I atom as a function of the I−CN_{COM} separation for the $^2\Sigma^+$-(X), $^2\Pi_{1/2}$-(A), and $^2\Sigma^+$-(B) states. A discussion of these states and their evaluation can be found elsewhere.[8,15] Briefly, we start by performing a multiconfiguration self-consistent field (MCSCF) calculation, followed by a multireference configuration interaction (MRCI) calculation. The states that form the active space for the MRCI calculation are then coupled by the spin−orbit Hamiltonian. All electronic structure calculations were carried out using the MOLPRO quantum chemistry package.[21] More details on the active space used in these calculations and the development of the potential surfaces can be found in Martin et al[8] and McCoy.[15]

An advantage of carrying out the electronic structure calculations in three steps is that it allows us to compare the energies and electronic wave functions that are generated in the MRCI calculations to those obtained once the spin−orbit coupling is introduced. From the fragment charges obtained for the states that result from the MRCI calculations, we find that the large change in the electronic structure of the spin−orbit coupled states near 4.5 Å is absent when the spin−orbit coupling is not included. This hints to the fact that we can use the MRCI states as a basis for a diabatic representation of the potentials. More specifically, looking at the decomposition of the spin−orbit coupled states in terms of the MRCI states, we found that only three states contribute to the potential curves that correlate to the $I^- + CN$ and $I^* + CN^-$ asymptotes.[8] The higher in energy of the two adiabatic states, the $^2\Sigma^+$-(B) state, is accessible by excitation in the UV, while the lower-energy state, the $^2\Pi_{1/2}$-(A) state is accessible by excitation in the 500-nm

region.[15] On the basis of this, we decouple the two adiabatic surfaces to generate a pair of diabatic states. More details on this procedure can be found in Martin et al.[8] It is important to note that the $^2\Pi$-(C) states are energetically close to the $^2\Sigma^+$-(B) state in the Franck−Condon region. As indicated above, in the linear geometry, and in the absence of spin−orbit coupling, most of the population would be excited to the $^2\Sigma^+$-(B) state. The introduction of spin−orbit coupling, and, more importantly, the lowered symmetry of ICN^- when it samples nonlinear geometries, provides parallel mechanisms for mixing between these states in the Franck−Condon window for UV excitation. This can be seen by the changing contribution of the $^2\Sigma^+$-(B) state and the $^2\Pi$-(C) states to the total transition moment as the anion is displaced from a linear geometry (see Supporting Information, Figure S1). Since the mixing is localized to the highly repulsive part of the potential, as we consider the potentials that are used to investigate the photodissociation dynamics of ICN^- following UV excitation, we treat the states that correlate to product channels (A) and (B) in a coupled diabatic representation, while the states that correlate to product channel (C) are treated as separate adiabatic potentials.
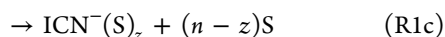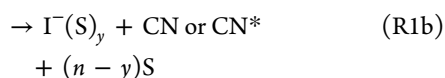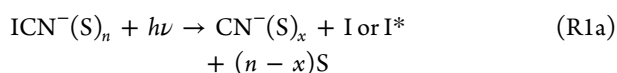
With the potentials in place, we perform quantum dynamics calculations of the UV photodissociation of bare ICN^- on diabatic potential-energy surfaces that correlate to product channels (A) and (B) and on the adiabatic potentials that correlate to product channel (C). The approach that is taken is similar to that of our visible ICN^-Ar_n study.[7] The surfaces employed are obtained from the electronic energies using the fitting procedure described elsewhere,[15] and are expressed in terms of the Jacobi Coordinates (R, θ): where R is the distance between the I atom and the center-of-mass of CN and θ is the angle between R and the CN bond. We define $\theta = 0°$ to be the linear ICN^- configuration and the INC^- configuration then corresponds to $\theta = 180°$. For the wavepacket calculations, we use the potential-energy surface of the ground state ($^2\Sigma^+$) to obtain the wave function that will be propagated. At $t = 0$, the initial wavepacket is promoted to the diabatic curves that correlates to product channel (A) (blue dashed curve in Figure 1a) or to one of the adiabatic curves that correlate to product channel (C), and the dynamics are followed as a function of time. (In all calculations, the C−N bond length is held constant at 1.16 Å.) We use a Lancozos scheme with 50 iterations for each 25-au time step to propagate the dynamics, with 2000 evenly spaced grid points in R(I-CN_{COM}) (ranging from 1.06 to 26.5 Å) and 150 grid points in θ (the zero's in the Legendre polynomials with l - m = 150).

From these calculations, we determine the theoretical branching percentages between the adiabatic ($I^* + CN^-$) and nonadiabatic ($I^- + CN$) dissociation channels. Additionally, we can evaluate the expectation values of the operators that make up the Hamiltonian to obtain the partitioning of the excess energy between translational and rotational degrees of freedom.

III. RESULTS AND DISCUSSION

We examine the UV-photodissociation dynamics of ICN^-, and the effects of solvation on these dynamics using two different solvents: S = Ar or CO_2. When considering the effects of solvation on the anion reaction dynamics, it is easiest to focus on a diabatic picture of the potential curves. In this diabatic picture, the charge varies smoothly along the reaction coordinate, which will give a more robust depiction of solvation. In the UV photodissociation of solvated ICN^-,

there are three general dissociation pathways detectable following excitation to the $^2\Sigma^+$ state:

$$ICN^-(S)_n + h\nu \rightarrow CN^-(S)_x + I \text{ or } I^* \quad \text{(R1a)}$$
$$+ (n - x)S$$

$$\rightarrow I^-(S)_y + CN \text{ or } CN^* \quad \text{(R1b)}$$
$$+ (n - y)S$$

$$\rightarrow ICN^-(S)_z + (n - z)S \quad \text{(R1c)}$$

Reaction R1a describes dissociation to form CN^--based products, whereas reaction R1b depicts a reaction that forms I^--based products. Lastly, reaction R1c shows solvent-induced recombination, which reforms stable ICN^--based products.

A. Wavelength-Dependence of ICN⁻ Photodissociation. Figure 2 displays the relative photodissociation cross
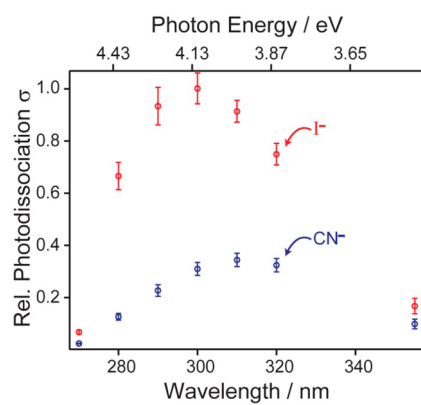
Figure 2. Relative ICN^- photodissociation cross sections for production of I^- (red) and CN^- (blue) between 270 and 355 nm. The maximum of the I^- relative cross section is set to unity. Each data point represents the average over 10 data sets, and the uncertainties are based on the standard deviation obtained from the 10 data sets averaged.

section of ICN^- obtained for detection of I^- (red) and CN^- (blue). The cross section obtained from detection of I^- reaches a maximum near 300 nm, while the CN^- cross section appears to peak at a slightly higher wavelength. The calculated potential-energy curves[15] of linear ICN^- (see Figure 1a) are in energetic agreement with the maximum in the cross section observed experimentally; the calculations suggest that this absorption feature is due to a $^2\Sigma^+ \leftarrow \tilde{X}\,^2\Sigma^+$ transition. Such a transition should result adiabatically in the production of CN^- and does not strictly agree with the large I^- intensities observed. As mentioned previously, it is possible to excite ICN^- to the $^2\Pi$ states as well as the $^2\Sigma^+$ states near the Franck–Condon window for UV excitation. For a strictly linear geometry, the transition moment to the $^2\Sigma^+$ state is an order of magnitude larger than the $^2\Pi$ states; however, for $\theta = 10°$, which is the most probable value for the ground-state wave function, the $^2\Pi$ states account for roughly one-third of the total transition moment. The contribution from these $^2\Pi$ states continues to rise and by $\theta = 30°$ it is almost equal to that of the $^2\Sigma^+$ state. (See Supporting Information, Figure S1.) The contribution of these higher-energy states accounts for some production of I^-, but still suggests that CN^- should be the dominant photoproduct. There is however, an additional source of the I^- product due to nonadiabatic transitions from

the $^2\Sigma^+$-(B) adiabatic state to the $^2\Pi_{1/2}$-(A) adiabatic state, which dissociates to produce $I^- + CN$.

Figure 3 displays the measured wavelength-dependent branching percentages of the ionic photoproducts for
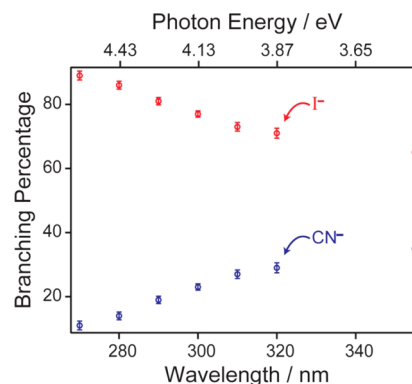
Figure 3. Branching percentages as a function of wavelength following UV photoexcitation of bare ICN^-. The I^- product is shown in red and the CN^- product in blue. Each point represents the average over 20 data sets, and the uncertainties are based only on the standard deviation obtained from the 20 data sets averaged.

dissociation of ICN^-. I^- is the dominant photoproduct over the entire wavelength region studied (270 to 355 nm). The CN^- photoproduct reaches its highest percentage at 355 nm, accounting for 35% of the total photoproducts. As the excitation wavelength decreases, the percentage of CN^- gradually decreases. At 300 nm (λ_{max}) the CN^- branching percentage has decreased to 23%, and by 270 nm (the lowest wavelength studied) it has diminished to roughly 10%.

The production of I^- is due in part to absorption to the $^2\Pi$-(C) states. Another route for producing I^- is by nonadiabatic transitions from the $^2\Sigma^+$-(B) adiabatic state to the $^2\Pi_{1/2}$-(A) adiabatic state. Quantum dynamics calculations were run on diabatic potential-energy surfaces for the states of ICN^- that dissociate to channels (A) and (B) to evaluate the branching into the $I^- + CN$ (nonadiabatic) channel following promotion of the ground-state wave function; an average branching of 24% is obtained for the nonadiabatic channel. Furthermore, the continued gradual decrease in the percentage of CN^- is in agreement with a simple Landau–Zener, two-state model.[22,23] In the Landau–Zener picture, the increasing excitation energy results in an increase in the anion velocity as it approaches the region of the avoided crossing and, thus, an increase in the probability for a nonadiabatic transition (producing I^-) and a decrease in the probability for adiabatic dissociation (producing CN^-). Such a trend is also seen when the calculated asymptotic wavepacket is projected onto momentum space. In this representation, we can analyze the branching as a function of the total energy. Over the range of experimentally accessed energies, the I^- channel corresponds to between 65% and 85% of the products, and the fraction increases with photon energy. This interpretation is incomplete, as the $^2\Pi$-(C) states are also accessible by UV excitation. It is likely that absorption to these $^2\Pi$-(C) states will also increase as the photon energy increases, thereby further increasing the amount of I^- produced. Yet, the experimental and theoretical results indicate the significance of nonadiabatic transitions in the UV-photodissociation dynamics of ICN^-.

B. Photodissociation of ICN⁻Ar$_n$, n = 0−5. The interaction energy between two Ar atoms is 12 meV,[24] and the binding energy of an Ar atom to ICN⁻ is about 50 meV.[25] The binding of one Ar atom to the anion is very labile,[26] and, for the small cluster sizes studied, we expect that additional Ar atoms will tend to clump together forming labile islands. While we do not expect the weak solvation energy to have much effect on the electronic structure of the anion in its equilibrium geometry, the presence of the solvent may well alter the dynamics, as solvation (approximated as a shifting of the diabatic states that correspond to the (A) and (B) asymptotes, plotted with dashed lines in Figure 1) will lead to a change in the value of R(I-CN$_{COM}$) where the two states cross, or, in some cases, remove the crossing entirely. In either case, it will alter the branching between the two product channels. Figure 4
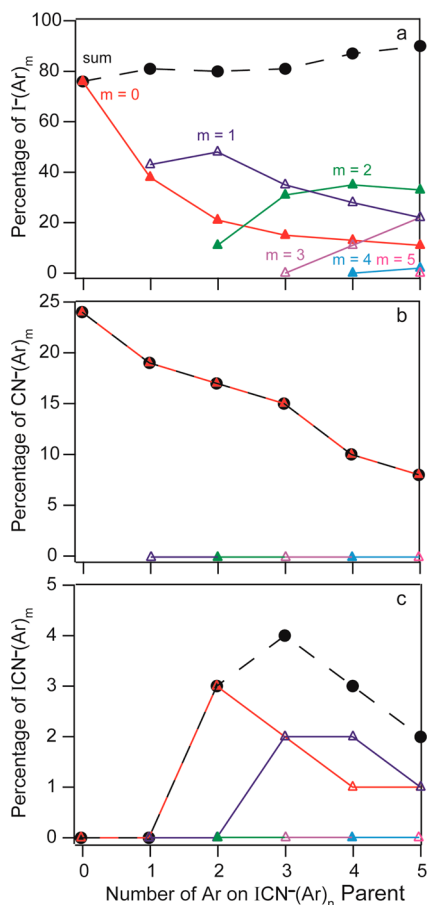

Figure 4. Branching percentages following UV photoexcitation of ICN⁻Ar$_n$, n = 0−5; numerical values can be found in Supporting Information, Table S1. Branching percentages of I⁻Ar$_m$ shown in (a), CN⁻Ar$_m$ shown in (b), and ICN⁻Ar$_m$ shown in (c). The total percentage of the given ionic photoproducts are given in black, while the various degrees of solvation are in color, keyed in (a).

shows the branching percentages for ICN⁻Ar$_n$ photodissociation using 300-nm (4.1-eV) light. Figure 4a displays the I⁻-based products, Figure 4b the CN⁻-based products, and Figure 4c the ICN⁻-based products. The total ionic photoproduct branching percentages (summed for all values of m: the number of solvent atoms that remain on the ionic photoproduct) are shown in dashed black lines, whereas each degree of solvation is shown in color, for example, m = 0 or no solvent retained on the product is shown in red.

The total ionic photoproduct percentages plotted as a function of parent cluster size in Figure 4 illustrate the effect of Ar solvation on the UV-photodissociation dynamics of ICN⁻. The addition of an Ar atom to ICN⁻ results in a slight decrease in the production of CN⁻-based products and, correspondingly, a slight increase in the production of I⁻-based products. Further addition of Ar atoms (n = 2, 3) results in a continued decrease in the percentage of CN⁻-based photoproducts. The percentage of I⁻-based photoproducts does not increase; instead, at n = 2 the recombination channel opens and ICN⁻ reforms. The total percentage of recombined products stays near 3% for the remainder of the cluster sizes studied. Nonetheless, the percentage of CN⁻-based photoproducts continues to decrease, thus when n = 4, 5 the percentage of I⁻-based photoproducts again increases. For all values of n, I⁻ is by far the dominate photoproduct. Similar changes to the product branching ratios were seen following visible excitation.[8]

In bare ICN⁻, I⁻ can be produced either from absorption to and direct dissociation on the ²Π-(C) states or by nonadiabatic dissociation on the ²Σ⁺-(B)state. The involvement of multiple states complicates the possible effects of Ar solvation on the dynamics. In general, solvation by Ar atoms will stabilize the anion because of the interaction of the solvent with the anion charge. As is seen in Figure 1b, depending on the electronic state and the I-CN$_{COM}$ separation, the excess charge may be on the I atom, the CN diatom, or shared between the two. Although the anion-Ar potential is rather flat, the interaction between the Ar atom and the CN⁻ is slightly stronger than the interaction with I⁻ or ICN⁻. On the basis of this, we approximate the effect of Ar solvation by lowering the energy of the diabatic potential that corresponds to the (B) asymptote, in which the excess charge localizes on the CN⁻ (green dashed line in Figure 1a) with respect to the diabatic potential that corresponds to the (A) asymptote, in which the charge localizes on the I⁻ (blue dashed line in Figure 1a). We then perform quantum dynamics calculations on bare ICN⁻, in which the (B)-diabatic state is lowered in energy to approximate the effects of Ar solvation on the dynamics. (Shifts of 50, 100, and 200 meV were used.) These calculations show an increase in the I⁻ product, in agreement with our experimental findings.

Inspecting the degree of solvation of the various ionic photoproducts further assists in our assessment of the dynamics. Figure 4 also reveals the presence of solvated I⁻-based photoproducts, but no solvation is observed for the CN⁻-based photoproducts. The Ar solvent is not strongly held to any particular location around ICN⁻, making solvation of either charged product possible. However, as will be described in more detail in Section III-D, the CN⁻ fragment acquires significant rotational energy and, in some cases, vibrational energy following UV excitation. Based on the wavepacket dynamics, the rotational energy is estimated to be roughly one-third of the available energy, while significant excitation of the CN stretch is expected following excitation to the ²Π-(C) states. While solvation of the CN⁻ fragment by Ar atoms is possible, with an average of roughly 0.83 eV of energy in CN⁻ rotation such complexes are not expected to live long enough to reach the detector intact.

The observation of recombined ICN⁻ is surprising; the asymptotic separation between the two ²Σ⁺ states is 0.94 eV[27] but the binding energy of the solvent is merely 0.05 eV. (Even for the anions that dissociate on the ²Π$_{1/2}$-(A) state, the asymptotic separation is still 0.80 eV.[27,28]) While the observation of ICN⁻ is surprising, the formation of ICN⁻Ar

from clusters originating with three to five Ar atoms is even more unexpected. Visible photodissociation studies found a steady recombination yield of roughly 6% for ICN⁻Ar₁₋₅, and these recombined products were also solvated.[7] The proposed mechanism for this recombination following visible excitation centers on the formation of an $[I^- - CN]$ complex on the $^2\Pi_{1/2}$ surface, following a substantial removal of available translational energy due to a CN-Ar collision and to a significant amount of energy in CN rotation. The formation of this complex allows sufficient time for radiative transfer back to the ground state, where stable ICN⁻ can reform. The UV photodynamics of ICN⁻ requires the loss of at least two Ar atoms for recombination to be observed, whereas only one Ar atom was required for this channel to be detected following visible excitation; yet with an additional 1.6 eV of available energy, the observation of caged products from the addition of two or more Ar atoms is remarkable. A radiative mechanism may also be important for these processes and will be discussed further in Section III-D.

C. Photodissociation of ICN⁻(CO₂)ₙ, n = 0−5. Based on MP2/6-311+G(2df) calculations, the interaction energy between two carbon dioxide molecules ranges between roughly 45 and 55 meV, and this value depends on the angle formed between the two monomers.[29] This stronger interaction along with the quadrupole-initiated preferential alignment of solvent molecules results in a more rigid structure than in the argon complexes. On the basis of charge density for the ground state of ICN⁻ (which is shared between the I atom and CN diatom) and previous studies of ICl⁻ and IBr⁻,[9,11,12] we expect the CO_2 solvent cage to initially form near the center of the I−CN bond in a geometry that has the two molecular axes roughly perpendicular to each other. Additional CO_2 molecules first form a ring around the ICN⁻ and then preferentially form around the smaller CN end of the anion. With a CO_2−ICN⁻ binding energy on the order of 250 meV,[8] the interaction between ICN⁻ and a CO_2 molecule is significantly greater than between ICN⁻ and an Ar atom, potentially having a larger effect on the electronically excited chromophore. The interaction between the anion and the solvent is dependent upon the geometry. While the structures of the clusters that are formed on the ground-state potential are dictated by the nature of these interactions, following photoexcitation, the additional solvent molecules may or may not be in a geometry that stabilizes the cluster relative to bare ICN⁻. As with Ar solvation, this effect can be modeled by lowering of the energy of the (B)-diabatic potential curves that lead to charge localization on the CN⁻ (green dashed line in Figure 1a) by a constant amount relative to the (A)-diabatic potential curves in which the charge localizes on the I⁻ (blue dashed line in Figure 1a). Figure 5 shows the branching percentages for ICN⁻(CO₂)ₙ photodissociation using 300-nm (4.1-eV) light. Figure 5a displays the I⁻-based products, Figure 5b the CN⁻-based products, and Figure 5c the ICN⁻-based products. Again, the total ionic photoproduct branching percentages are shown in dashed black lines and each degree of solvation is shown in color.

The total ionic photoproduct percentages plotted as a function of parent-cluster size in Figure 5 illustrate the effect of CO_2 solvation on the UV-photodissociation dynamics of ICN⁻. As with Ar solvation, the addition of a single CO_2 molecule results in a slight increase in the I⁻-based products. However, for n = 3−5 the percentage of I⁻-based products decreases and the percentage of CN⁻-based products and ICN⁻-based products increases. The initial trend follows the expected

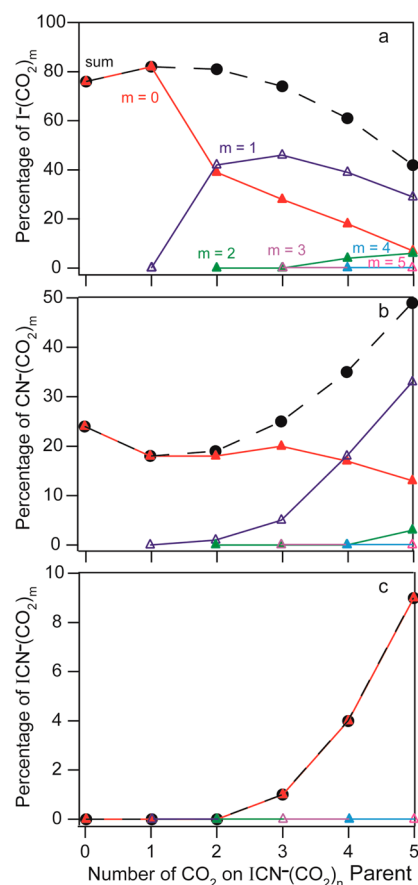**Figure 5.** Branching percentages following UV photoexcitation of ICN⁻(CO₂)ₙ, n = 0−5; numerical values can be found in Supporting Information, Table S2. Branching percentages of $I^-(CO_2)_m$ shown in (a), $CN^-(CO_2)_m$ shown in (b), and $ICN^-(CO_2)_m$ shown in (c). The total percentage of the given ionic photoproducts are given in black, while the various degrees of solvation are in color, keyed in (a).

behavior, as solvation should lower the diabatic state that correlates to asymptote (B) with respect to the one that correlates to asymptote (A). The decrease in the percentage of I⁻ for n = 3−5 hints at the fact that this simple picture is incomplete in the case of CO_2 solvation.

Another factor that dictates the production of I⁻- versus CN⁻-based products, and which is not included in this simplified model, is the ability of CN⁻ and CO_2 to react, forming the $[NCCO_2]^-$ molecular anion.[8,14] Competition to form this stable anion is likely the reason there is a decrease in the I⁻-based products. Figure 5 also displays the degree of solvation obtained for the products. Following photoexcitation of ICN⁻(CO₂)ₙ, the I⁻-based photoproducts show a smaller degree of solvation. As described above,[30−32] it is expected that the more rigid CO_2 solvent cage forms initially near the center of the I−CN bond and then preferentially around the CN in the ground electronic state. This geometry makes it more likely that the CO_2 molecules will solvate the CN⁻ product than the I⁻ product following photoexcitation. Additionally, we find that CO_2 solvation of the CN⁻-based photoproducts is higher than in the case of Ar solvation. While, the solvent-anion geometry favors such a finding there is also the matter of CN rotation. Again, there is an average of roughly 0.83 eV of energy in CN⁻ rotation, and a CN⁻(CO₂) complex is not expected to live long enough to reach the detector intact; but, there is the additional driving force for solvation of this fragment due to the formation

of the $[NCCO_2]^-$ molecular anion.[8,14] Having solvent evaporation to dissipate excess energy, the $CN^-(CO_2)$ complex can react to form the $[NCCO_2]^-$ molecular anion. Interestingly, the onset of solvated CN^--based photoproducts resembles the onset of recombined products. Since the $[NCCO_2]^-$ and ICN^- molecular anions have similar dissociation energies (~ 0.8 eV[8,14] and 0.83 eV,[25] respectively), it is perhaps not surprising that these two anions would require a similar number of solvent molecules to stabilize their formation.

Also apparent in Figure 5 is a small and slowly increasing percentage of ICN^- formed; and, these recombined products only form bare. Recombination is first observed at $n = 3$, which is close to the number of solvent molecules expected to close the energy gap between the ground and excited states. While the percentage of recombined products does increase with an increase in n, recombination remains a very minor channel only reaching 9% of the total ionic photoproducts for $n = 5$. The increase in production of ICN^- with an increase in the parent cluster size is unlike the roughly constant 3% recombination yield observed for UV photodissociation of ICN^-Ar_n. Likewise, there is no $ICN^-(CO_2)$ detected for any of the cluster sizes studied, but there is production of ICN^-Ar following 4.1-eV excitation of ICN^-Ar_{3-5}. The differing recombination results, namely, the degree of solvation of the recombined products and the variance of the recombination percentage as a function of the parent cluster size, indicate distinct mechanisms for recombination in the UV photodissociation of ICN^-Ar_n and $ICN^-(CO_2)_n$. These results mirror those of the visible photodissociation of ICN^-Ar_n[7] and $ICN^-(CO_2)_n$[8] suggesting that when solvated by CO_2 recombination of ICN^- occurs following nonadiabatic transitions to the ground state, while recombination of ICN^- solvated by Ar atoms occurs following radiative transfer to the ground state.

D. Analysis of Energy Partitioning and Recombination of ICN^-. The UV photodissociation of partially solvated ICN^- results in the reformation of ICN^- with the addition of two Ar atoms or three CO_2 molecules to the parent anion. Given the roughly 1-eV mismatch in the asymptotic regions of the $^2\Sigma^+$-(X) ground state and $^2\Sigma^+$-(B) excited state potentials, it would take roughly four CO_2 molecules or twenty Ar atoms to consider solvent-induced transitions to the ground state. As discussed in Sections III−B and III−C, recombination of $ICN^-(CO_2)_n$ following UV excitation likely occurs by means of such a mechanism, but recombination of ICN^-Ar_n following UV excitation requires an alternate mechanism. In our visible study on ICN^-Ar_n we observed one-atom caging,[7] for which we proposed a radiative mechanism. The model employs a CN-Ar collision to reduce the excess translational energy remaining within the I^- and CN components, along with populating a reasonable degree of rotational excitation in the CN fragments. Together, these processes tie up a considerable amount of energy permitting an $[I^-−CN]$ complex with a sufficient excited-state lifetime to allow for a non-negligible radiative transition probability.

In the case of recombination following visible excitation, trapping of an $[I^-−CN]$ complex occurs on the $^2\Pi_{1/2}$-(A) surface. Following UV excitation, both the $^2\Pi_{1/2}$-(A) and $^2\Pi$-(C) surfaces are accessible. We can address the feasibility of a similar mechanism in the UV photodissociation of ICN^-Ar_n, $n = 2−5$. A collision between the departing CN diatom and one Ar solvent atom can reverse the CN trajectory, sending it back toward the I^-Ar_m. The key is to determine if there are ways to dissipate enough energy to trap an $[I^-−CN]$ complex on either

the $^2\Pi_{1/2}$-(A) or $^2\Pi$-(C) surfaces. Using a simple hard-sphere model that only considers translational degrees of freedom, we determine the kinematics of a collinear CN−Ar collision as detailed in the Supporting Information. For dissociation events occurring on both the $^2\Pi_{1/2}$-(A) excited state and the $^2\Pi$-(C) excited states, a simple kinematic model is insufficient to explain the observed recombination.

By performing quantum dynamics calculations of the UV photodissociation of bare ICN^- on potential-energy surfaces for the $^2\Pi_{1/2}$-(A) excited state and the $^2\Pi$-(C) excited states with fixed CN bond lengths, we estimate the fractional partitioning of the excess energy between translational and rotational degrees of freedom. These calculations show that roughly one-third of the available energy ends up in CN rotation. While these numbers show efficient translational to rotational energy transfer, the energetics still indicate that an $[I^-−CN]$ complex will dissociate on both the $^2\Pi_{1/2}$-(A) excited state and the $^2\Pi$-(C) excited states.

In addition, when we consider how the CN stretch potential is altered by excitation to the $^2\Pi_{1/2}$-(A) and $^2\Pi$-(C) excited states, we find a shift in the minimum energy CN distance of roughly 0.045 Å on the $^2\Pi$-(C) excited states compared to the minimum on the ground-state potential. In the harmonic approximation, this leads to a prediction that one-third of the CN* formed following dissociation on the $^2\Pi$-(C) states has at least one quantum of vibrational excitation, and the $v = 2$ level is excited in 6% of the cases. Such CN vibrational excitation is not expected following excitation to the other states depicted in Figure 1a.

When considering the possibility of CN stretching excitation on the $^2\Pi$-(C) states, it is found that for anions having two quanta excited, roughly 40% of the excess energy must be deposited into CN rotation to trap an $[I^-−CN]$ complex; for one quantum of excitation, roughly 45% of the excess energy must be tied up in CN rotation. Quantum dynamics calculations determine that for excitation of the rovibronic ground state of bare $^2\Sigma^+$-(X) ICN^- to the $v = 0$ level of the $^2\Pi$-(C) states, between 33% and 37% of the excess energy goes into excitation of the CN rotor. Moreover, population of the low-frequency bending vibration (70 cm^{-1})[15] of ICN^- is expected in our anion beam, and calculations on the $^2\Pi_{1/2}$-(A) surface showed that bending excitation results in an increase in the fraction of the excess energy stored in rotation of the CN moiety. Thus, the dissociation of CN-stretch excited anions on the $^2\Pi$-(C) surfaces provide a plausible mechanism for the recombination observed following UV excitation.

IV. SUMMARY

The dynamics of mass-selected ICN^-Ar_n and $ICN^-(CO_2)_n$, $n = 0−5$, are monitored following UV photodissociation. The relative photodissociation cross sections are recorded for bare ICN^- by detection of the I^- and CN^- photoproducts. The relative photodissociation cross sections, as well as the wavelength-dependent branching percentages, reveal a dominance of the I^- photoproduct over the entire wavelength range studied: 270 to 355 nm. The absorption is due in part to the $^2\Sigma^+ \leftarrow \tilde{X}\ ^2\Sigma^+$ transition, which should produce CN^-; however, following absorption some of the photoexcited anions undergo a nonadiabatic transition from the $^2\Sigma^+$ state to the $^2\Pi_{1/2}$ state thus producing I^-. The other contribution to the I^- signal is due to absorption to the $^2\Pi$ states that produce $I^- + CN^*$. Partial solvation of ICN^- to form ICN^-Ar_n and $ICN^-(CO_2)_n$, $n = 1−5$, influences the dynamics between the dissociation

channels that produce CN$^-$-based products (I* + CN$^-$) and I$^-$-based products (I$^-$ + CN or I$^-$+ CN*). In the case of Ar solvation, there is a steady increase in the production of I$^-$-based products as n increases from 1 to 5; conversely, with CO_2 solvation, the addition of one or two solvent molecules decreases the formation of CN$^-$-based products but three, four, and five solvent molecules results in an increase in the percentage of CN$^-$-based products formed. With solvation an increase in the I$^-$-based products is anticipated; for CO_2 solvation, the subsequent decrease in the I$^-$-based products is likely due to the formation of a $[NCCO_2]^-$ molecular anion. Recombination occurs with the addition of two Ar atoms or three CO_2 molecules; recombination of ICN$^-$(CO_2)$_n$ and ICN$^-$Ar$_n$ occur via different mechanisms. The nonadiabatic recombination mechanism proposed for recombination in the UV photodissociation of ICN$^-$(CO_2)$_n$, n = 3–5, is analogous to previous studies of cluster anions whereby solvation induces nonadiabatic transitions to high-lying levels of the ground state, followed by stabilization through solvent evaporation. The mechanism for recombination in the UV photodissociation of ICN$^-$Ar$_n$, n = 2–5, is uncertain, though it likely involves trapping on the excited $^2\Pi$-(C) surfaces followed by a radiative transition.

ASSOCIATED CONTENT

Ⓢ Supporting Information

The supporting information contains the calculated total transition moment, the full breakdown of the photoproduct branching percentages for ICN$^-$Ar$_n$ and ICN$^-$(CO_2)$_n$, and the energetic breakdown for recombination following UV excitation of ICN$^-$Ar$_n$. This material is available free of charge via the Internet at http://pubs.acs.org.

AUTHOR INFORMATION

Corresponding Author
*E-mail: mccoy@chemistry.ohio-state.edu (A.B.M.), wcl@jila.colorado.edu (W.C.L.).

Present Address
§Department of Chemistry, University of Wisconsin-Madison, Madison, WI 53706.

Notes
The authors declare no competing financial interest.

ACKNOWLEDGMENTS

REFERENCES

(1) Black, J. F.; Waldeck, J. R.; Zare, R. N. Evidence for Three Interacting Potential Energy Surfaces in the Photodissociation of ICN at 249 nm. *J. Chem. Phys.* **1990**, *92*, 3519–3538.

(2) Nadler, I.; Mahgerefteh, D.; Reisler, H.; Wittig, C. The 266 nm Photolysis of ICN: Recoil Velocity Anisotropies and Nascent E,V,R,T Excitations for the CN+I(^{2}P$_{3/2}$) and CN+I(^{2}P$_{1/2}$) Channels. *J. Chem. Phys.* **1985**, *82*, 3885–3893.

(3) Amatatsu, Y.; Yabushita, S.; Morokuma, K. Ab Initio Potential Energy Surfaces and Trajectory Studies of A-Band Photodissociation Dynamics: ICN* –> I+CN and I*+CN. *J. Chem. Phys.* **1994**, *100*, 4894–4909.

(4) Qian, J.; Tannor, D. J.; Amatatsu, Y.; Morokuma, K. Ab Initio Structure and Wave Packet Dynamics of ICN Photodissociation. *J. Chem. Phys.* **1994**, *101*, 9597–9609.

(5) Moskun, A. C.; Bradforth, S. E. Photodissociation of ICN in Polar Solvents: Evidence for Long Lived Rotational Excitation in Room Temperature Liquids. *J. Chem. Phys.* **2003**, *119*, 4500–4515.

(6) Rivera, C. A.; Winter, N.; Harper, R. V.; Benjamin, I.; Bradforth, S. E. The Dynamical Role of Solvent on the ICN Photodissociation Reaction: Connecting Experimental Observables Directly with Molecular Dynamics Simulations. *Phys. Chem. Chem. Phys.* **2011**, *13*, 8269–8283.

(7) Case, A. S.; Miller, E. M.; Martin, J. P.; Lu, Y.-J.; Sheps, L.; McCoy, A. B.; Lineberger, W. C. Dynamic Mapping of CN Rotation Following Photoexcitation of ICN$^-$. *Angew. Chem., Int. Ed.* **2012**, *124*, 2651–2653.

(8) Martin, J. P.; Case, A. S.; Gu, Q.; Darr, J. P.; McCoy, A. B.; Lineberger, W. C. Photofragmentation Dynamics of ICN$^-$(CO_2)$_n$ Clusters Following Visible Excitation. *J. Chem. Phys.* **2013**, submitted 5/2013; MS# A13.05.0035.

(9) Nadal, M. E.; Kleiber, P. D.; Lineberger, W. C. Photofragmentation of Mass-Selected ICl$^-$(CO_2)$_n$ Cluster Ions: Solvation Effects on the Structure and Dynamics of the Ionic Chromophore. *J. Chem. Phys.* **1996**, *105*, 504–514.

(10) Vorsa, V.; Nandi, S.; Campagnola, P. J.; Larsson, M.; Lineberger, W. C. Recombination Dynamics Of Photodissociated I$_2$$^-$ In Size-Selected Ar and CO_2 Clusters. *J. Chem. Phys.* **1997**, *106*, 1402–1410.

(11) Sanford, T. J.; Han, S.-Y.; Thompson, M. A.; Parson, R.; Lineberger, W. C. Photodissociation Dynamics of IBr$^-$(CO_2)$_n$, n < 15. *J. Chem. Phys.* **2005**, *122*, 054307.

(12) Dribinski, V.; Barbera, J.; Martin, J. P.; Svendsen, A.; Thompson, M. A.; Parson, R.; Lineberger, W. C. Time-Resolved Study of Solvent-Induced Recombination in Photodissociated IBr$^-$(CO_2)$_n$ Clusters. *J. Chem. Phys.* **2006**, *125*, 133405.

(13) Klots, C. E. The Evaporative Ensemble. *Z. Phys. D: At., Mol. Clusters* **1987**, *5*, 83.

(14) Larson, J. W.; Szulejko, J. E.; McMahon, T. B. Gas-Phase Lewis Acid-Base Interactions - An Experimental-Determination of Cyanide Binding-Energies from Ion-Cyclotron Resonance and High-Pressure Mass-Spectrometric Equilibrium Measurements. *J. Am. Chem. Soc.* **1988**, *110*, 7604–7609.

(15) McCoy, A. B. Potential Energy Surfaces and Porperties of ICN$^-$ and ICN. *Int. J. Quantum Chem.* **2013**, *113*, 366–74.

(16) Thompson, M. A.; Martin, J. P.; Darr, J.; Lineberger, W. C.; Parson, R. A Combined Experimental/Theoretical Investigation of the Near-Infrared Photodissociation of IBr$^-$(CO_2)$_n$. *J. Chem. Phys.* **2008**, *129*, 224304.

(17) Boo, D. W.; Ozaki, Y.; Andersen, L. H.; Lineberger, W. C. Femtosecond Dynamics of Linear Ag$_3$$^-$. *J. Phys. Chem. A* **1997**, *101*, 6688–6696.

(18) Sanford, T. J.; Han, S.-Y.; Thompson, M. A.; Parson, R.; Lineberger, W. C. Photodissociation Dynamics of IBr$^-$(CO_2)$_n$, n < 15. *J. Chem. Phys.* **2005**, *122*, 054307.

(19) Bak, B.; Hillebert, A. Cyanogen Iodide. *Org. Synth.* **1963**, *4*, 207.

(20) Wiley, W. C.; McLaren, I. H. Time-of-Flight Mass Spectrometer with Improved Resolution. *Rev. Sci. Instrum.* **1955**, *26*, 1150–57.

(21) Werner, H.-J.; Knowles, P. J.; Knizia, G.; Manby, F. R.; Schütz, M.; Celani, P.; Korona, T.; Lindh, R.; Mitrushenkov, A.; Rauhut, G., et al. MOLPRO, a Package of Ab Initio Programs, Version 2002.6; 2003.

(22) Landau, L. D. On the Theory of Transfer of Energy at Collisions II. *Phys. Z. Sowjetunion* **1932**, *2*, 46.

(23) Zener, C. Non-Adiabatic Crossing of Energy Levels. *Proc. R. Soc. London, A* **1932**, *137*, 696.

(24) Herman, P. R.; LaRocque, P. E.; Stoicheff, B. P. Vacuum Ultraviolet-Laser Spectroscopy 0.5. Rovibronic Spectra of Ar$_2$ and Constants of the Ground and Excited-States. *J. Chem. Phys.* **1988**, *89*, 4535–49.

(25) Miller, E. M.; Sheps, L.; Lu, Y.-J.; Case, A. S.; McCoy, A. B.; Lineberger, W. C. New View of ICN A Continuum Using Photoelectron Spectroscopy of ICN⁻. *J. Chem. Phys.* **2012**, *136*, 044313.

(26) Martin, J. P. Photofragmentation and Recombination Dynamics of Partially-Solvated Anionic Clusters. Ph.D. Thesis, University of Colorado, Boulder, CO, 2012.

(27) Moore, C. E., *Atomic Energy Levels*, 2nd ed.; National Bureau of Standards: Washington, DC, 1971; Vol. 35.

(28) Bradforth, S. E.; Kim, E. H.; Arnold, D. W.; Neumark, D. M. Photoelectron Spectroscopy of CN⁻, NCO⁻, and NCS⁻. *J. Chem. Phys.* **1993**, *98*, 800−810.

(29) Tsuzuki, S.; Uchimaru, T.; Mikami, M.; Tanabe, K. Intermolecular Interaction Potential of the Carbon Dioxide Dimer. *J. Chem. Phys.* **1998**, *109*, 2169−2175.

(30) Faeder, J.; Delaney, N.; Maslen, P. E.; Parson, R. Modeling Structure and Dynamics of Solvated Molecular Ions: Photodissociation and Recombination in $I_2^-(CO_2)_n$. *Chem. Phys.* **1998**, *239*, 525−547.

(31) Maslen, P. E.; Faeder, J.; Parson, R. An Effective Hamiltonian for an Electronically Excited solute in a Polarizable Molecular Solvent. *Mol. Phys.* **1998**, *94*, 693−706.

(32) Parson, R.; Faeder, J.; Delaney, N. Charge Flow and Solvent Dynamics in the Photodissociation of Solvated Molecular Ions. *J. Phys. Chem. A* **2000**, *104*, 9653−9665.